Chemical Engineering Journal Advances 9 (2022) 100198

Contents lists available at ScienceDirect

Chemical Engineering Journal Advances

journal homepage: www.sciencedirect.com/journal/chemical-engineering-journal-advances

Effective degradation of cyclohexanecarboxylic acid by visible LED driven photo-Fenton

Alicia L. Garcia-Costa *, Lucia Lopez-Perela, Gema Pliego, Juan A. Zazo, Jose A. Casas

Chemical Engineering Department, School of Science, Universidad Autonoma de Madrid, Ctra. Colmenar Viejo km. 15, 28049, Madrid, Spain

ARTICLE INFO

Keywords:
Naphthenic acids
Advanced oxidation
Process intensification
Wastewater treatment

ABSTRACT

This work explores the feasibility of visible LEDs (λ: 400–800 nm) used in photo-Fenton for the degradation of a 50 mg/L cyclohexanecarboxylic acid (CHA) as model naphthenic acid present in process wastewater from the oil sands industry. The influence of initial pH, catalyst concentration and iron oxidation state, H_2O_2 dose and radiant flux were studied. In all trials, an initial lag phase in both the H_2O_2 decomposition and TOC evolution was observed. This seems to be related to the generation of a complex between CHA, hydrogen peroxide and iron (CHA-H_2O_2-Fe). This iron scavenging decreases the H_2O_2 decomposition rate, leading to a lagged mineralization kinetics. Nonetheless, process intensification using visible radiation (λ_{max}: 460 nm) favors the CHA-H_2O_2-Fe photoactivation and breakdown when using an H_2O_2 concentration higher than 33% of the stoichiometric dose for complete CHA mineralization. Under the optimum conditions pH_0 3, Φ: 280 W/m^2, Fe^{2+}:20 mg/L and H_2O_2: 144 mg/L, which corresponds to 60% of the stoichiometric amount, 75% of TOC removal was achieved.

1. Introduction

Given the rising demand of fuel and the wide exploitation of conventional crude reservoirs, over the past decades non-conventional crude sources, like oil sands, have increased their production [1]. The separation of the heavy crude, also known as bitumen, from the sands requires the use of 1.4 m^3 water per barrel of produced oil. During the separation process, both inorganic and organic components are transferred to the aqueous phase, which is also referred as oil sands produced water (OSPW) [2]. These OSPW cannot be reused in the separation process due to the saline content and the must not discharged into the environment, due to their organic charge and toxicity. Hence, they are accumulated in vast tailing ponds. The latest report from the Natural Resources Defense Council (NRDC) estimated the total volume of wastewater in 1.18 trillion liters in 2017 [3]. Thus, efficient technologies must be developed for the remediation of these highly polluted wastewater.

Among the organic fraction in OSPW, naphthenic acids (NAs) stand out due to the toxicity that they confer to these effluents [4]. These NAs belong to a complex group of carboxylic acids, organic and polar, that occur naturally in hydrocarbon deposits (petroleum, oil sands, crude oil and bitumen). They have been a concern since the late 20th century for being corrosive to pipelines and equipment in refineries. OSPW usually present concentrations of NAs in the range of 40–120 mg/L [5].

So far, several methods have been developed for the removal of NAs, such as adsorption [6–8] or membrane filtration [9–11]. Nonetheless, these technologies only transfer the pollutants without transforming them, generating more hazardous waste streams. Therefore, other technologies, such as Advanced Oxidation Processes (AOPs) represent an interesting alternative, since they are highly effective for the mineralization of organic pollutants [12]. AOPs involve the generation of highly oxidizing species, such as hydroxyl radicals ($HO^{\bullet}$), which are highly-reactive and non-selective, being able to oxidize a wide variety of organic pollutants. Several AOPs have been applied for NAs removal in aqueous phase [13], such as catalytic ozonation [14], chlorine-based processes [15, 16], persulfate oxidation [17, 18] and H_2O_2-based processes [16, 19]. Amongst these, H_2O_2-based processes are the most interesting, since this oxidant is environmentally friendly as it yields H_2O and O_2. On the other hand, ozone (O_3) presents promising results but it is a toxic gas which should be handled with care; chlorination may yield very toxic reaction intermediates [20] and persulfate increases the water salinity, as it decomposes towards sulfate.

Among the H_2O_2-based AOPs, the Fenton process is especially relevant because of its high efficiency, high availability of reagents and simple equipment requirements. This technology consists of redox cycle using an iron salt as catalyst in acidic media. In the process, H_2O_2 acts as

* Corresponding author.
E-mail address: alicial.garcia@uam.es (A.L. Garcia-Costa).

https://doi.org/10.1016/j.ceja.2021.100198
Received 25 September 2021; Received in revised form 26 October 2021; Accepted 29 October 2021
Available online 3 November 2021

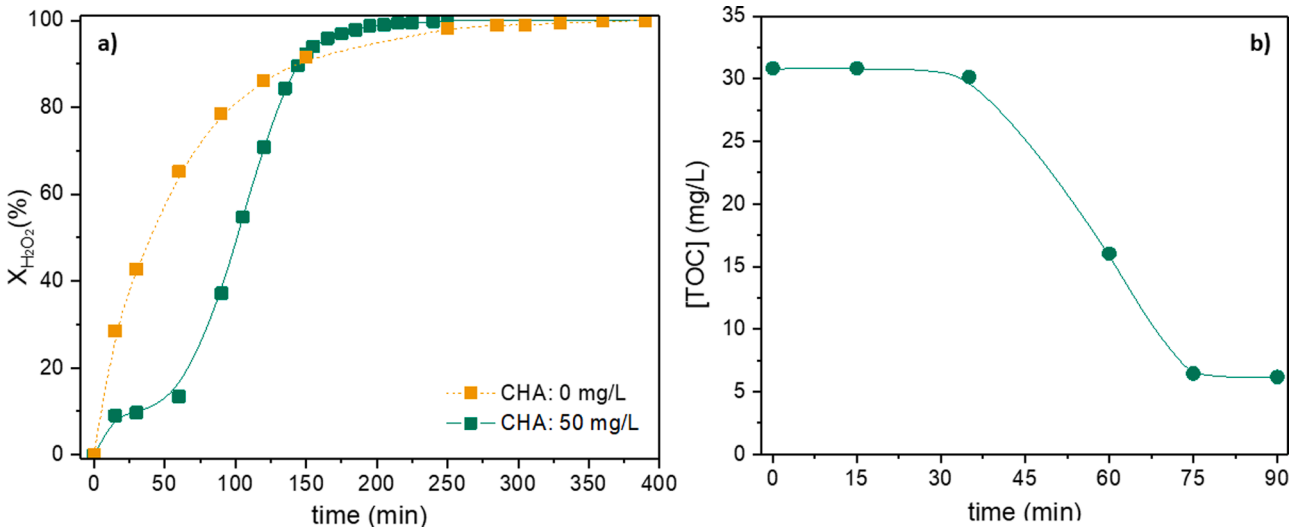

Fig. 1. a) H_2O_2 conversion and b) TOC evolution in CHA photo-Fenton oxidation. Experimental conditions: $[CHA]_0$ = 50 mg/L; $[CHA]_0$ = 0 mg/L; $[H_2O_2]_0$ = 239 mg/L; $[Fe^{2+}]$=10 mg/L; 280 W/m^2 irradiance; pH_0=3; T = 25 °C; r_{agit}:250 rpm.

both oxidant and reducing agent, yielding both $HO^{\bullet}$ and hydroperoxide ($HOO^{\bullet}$) radicals, respectively, as shown in Eqs (1) and 2 [21]. These radicals are the responsible for organic matter depletion due to their high oxidation potential ($E^0_{HO\bullet}$: +2.74 V. $E^0_{HOO\bullet}$: +1.70 V) [22].

$$Fe^{2+} + H_2O_2 \rightarrow Fe^{3+} + HO^{\bullet} + OH^- \quad \text{(Eq. 1)}$$

$$Fe^{3+} + H_2O_2 \rightarrow Fe^{2+} + HOO^{\bullet} + H^+ \quad \text{(Eq. 2)}$$

One of the main drawbacks of this process is related to radical scavenging, a phenomenon that occurs because of nonselective nature of $HO^{\bullet}$. This hinders the efficiency of the process since they can interact not only with the organic contaminants but also with inorganic constituents such as carbonates, or even with other radicals, in the so-called auto-scavenging reactions, yielding H_2O_2 or H_2O Eqs (3)-(4)

$$HO^{\bullet} + HO^{\bullet} \rightarrow H_2O_2 \quad \text{(Eq. 3)}$$

$$HO^{\bullet} + HO_2^{\bullet} \rightarrow H_2O + O_2 \quad \text{(Eq. 4)}$$

Combination of H_2O_2 and Fe^{2+} with UV–vis radiation is known as photo-Fenton. In this process, light incidence enhances the reduction of Fe^{3+} to Fe^{2+} (Eq. (5)). Furthermore, there is an additional radical generation by H_2O_2 photolysis (Eq. (6)). Hence, the intensification of the Fenton process by UV radiation results in greater reaction rates and increased pollutant depletion [23, 24].

$$Fe^{3+} + H_2O + h\upsilon \rightarrow Fe^{2+} + HO^{\bullet} + H^+ \quad \text{(Eq. 5)}$$

$$H_2O_2 + h\upsilon \rightarrow HO^{\bullet} + HO^{\bullet} \quad \text{(Eq. 6)}$$

Photo-Fenton has thoroughly been studied using UV radiation despite the fact that using UV lamps increases importantly the cost of photo-Fenton process. In this sense, light-emitting diodes (LED) turn out as a feasible alternative because of their continuous supply and lower energy requirement [25, 26].

Regarding the degradation of naphthenic acids by photo-Fenton, Zhang et al. explored the degradation of cyclohexanecarboxylic acid (CHA) using a medium-pressure Hg lamp [27]. Complete CHA transformation was reached after 18 min working at $[CHA]_0$ = 50 mg/L, $[H_2O_2]_0$ = 50 mg/L and $[Fe^{2+}]$=5 mg/L. Nonetheless, this work only reveals the fate of the starting pollutant and the hydrogen peroxide. Without further information on the Total Organic Carbon (TOC) it is not possible to determine whether there is an efficient mineralization of CHA or a mere transformation into another species. Besides, the use of UV-C lamps, which have a higher energy consumption, may compromise the feasibility of the process. Hence, this work aims to employ for the first time a vis-LED assisted Fenton process for the degradation of CHA, evaluated in terms of TOC depletion. Furthermore, the influence of several operating conditions such as pH, catalyst concentration and iron oxidation state, H_2O_2 dose and irradiance on CHA depletion are evaluated to gain a deeper comprehension on the mineralization process.

2. Materials and methods

2.1. Reactants

Cyclohexanecarboxylic acid (CHA, 98%), $FeCl_2$ (98%) and $FeCl_3$ (97%) were supplied by Sigma-Aldrich and H_2O_2 (30% w/v) by Panreac. All aqueous solutions for reaction were prepared at pH_0 3.0 ± 0.1 using HCl (37% w/v; Panreac) in ultrapure water.

H_3PO_4 (85 wt.%), o-phenanthroline (≥ 99%), hydroxylamine hydrochloride (99%) and $TiOSO_4$ (1.9–2.1%), supplied by Sigma-Aldrich, were used in the analytic procedure. All reagents were of analytical grade and were used as received without further purification. Ultrapure water was used throughout the work. Synthetic OSPW was prepared by addition of NaCl (≥ 99%), Na_2SO_4 (≥ 99%), and Na_2CO_3 (≥ 99.5%), provided by Sigma-Aldrich.

2.2. Photo-Fenton experiments

Experiments were carried out in a 500 mL Pyrex jacketed glass batch reactor equipped with a visible LED lamp situated 1 cm above the reactor. The lamp has 72 phosphor-converted white LEDs; 5500 K; I: 280 W/m^2; λ: 400–800 nm, λ_{MAX}: 460 nm. Full characterization of the lamp and the emission spectra is published elsewhere [24].

In a typical reaction 295 mL of CHA 50 mg/L and 10 mg/L Fe^{2+} were introduced in the reactor and stirred at 250 rpm. Afterwards, the lamp was turned on and 5 mL of an H_2O_2 aqueous solution was introduced, representing the start of the reaction. Temperature was kept at 25ºC using a thermal bath recirculation system (Julabo 13). All experiments were performed three times, with a statistical deviation in the results lower than 5% in all cases.

2.3. Analytical methods

Samples were periodically taken from the reactor and were immediately analyzed. Total organic carbon (TOC) was measured in a TOC analyzer (Shimadzu, model TOC VSCH), H_2O_2 was determined by

colorimetric titration using the $TiOSO_4$ method [28] and dissolved iron was determined by colorimetric titration using o-phenanthroline method [29].

2.4. Determination of apparent rate constants

Pseudo-first order apparent kinetic constants for H_2O_2 decomposition were calculated by linear regression using OriginPro 2017 software. The lag phase was not included in the analysis, using as initial point the last data in the initial plateau observed prior to the decay in H_2O_2 decomposition.

3. Results and discussion

3.1. Initial runs

CHA degradation was firstly studied by means of photolysis, Vis-LED/H_2O_2,Fenton and photo-Fenton working at 50 mg/L CHA, 239 mg/L H_2O_2 (which corresponds to the stoichiometric dose required for complete CHA mineralization) and 10 mg/L Fe^{2+}. Results are depicted in Figure S1 of the Supporting Information (SI), where a negligible CHA mineralization was reached after 90 min in the photolysis, Vis-LED/H_2O_2 and dark Fenton runs. This was ascribed to the use of a vis-LED source, which cannot carry out the CHA or H_2O_2 photolysis, in the case of the photo-assisted runs.

When the dark-Fenton run was prolonged to 900 min the TOC value decreased by 50.2%. This represents an average mineralization rate, defined as the quotient between converted TOC and the reaction time as shown in Eq. (7), of $-\overline{r_{TOC}}$: 0.02 mg/L·min. On the other hand, the photo-Fenton run yielded a 79.8% TOC abatement in only 240 min and $-\overline{r_{TOC}}$: 0.11 mg/L·min, five times faster.

$$(-\overline{r_{TOC}}) = \frac{C_{TOC,0} - C_{TOC,\ t}}{t} \quad \text{(Eq. 7)}$$

To gain a deeper comprehension on the reaction system, H_2O_2 evolution in photo-Fenton was evaluated in presence and absence of CHA, as shown in Fig. 1a. H_2O_2 decomposition reaction follows a pseudo-first kinetic order with an apparent rate constant of $k_{app,H2O2}$: 1.59×10^{-2} min^{-1} at 25 °C (r^2=0.99) in absence of CHA. When CHA is present in the system a lag phase may be observed in the first 40 min of reaction. During this period, H_2O_2 decomposition rate is roughly zero, but once its decomposition starts, the rate constant is higher than the one of the system in which no CHA was added ($k_{app,H2O2}$: 2.09×10^{-2} min^{-1}, r^2: 0.98). This is due to the oxidation of organics which may yield organic radicals, as depicted in Eq. (8) and 9, which are also involved in the consumption of hydrogen peroxide [30–32].

$$RH + HO^{\bullet} \rightarrow R^{\bullet} + H_2O \quad \text{(Eq. 8)}$$

$$R^{\bullet} + H_2O_2 \rightarrow ROH + HO^{\bullet} \quad \text{(Eq. 9)}$$

The same lag phase for H_2O_2 consumption was also observed in the TOC evolution, as can be seen in Fig. 1b. It is widely known that naphthenic acids are corrosive in refineries due to the formation of iron naphthenates according to Eq. (10), where RCOOH represents a generic naphthenic acid [33]. This scavenging process has also been reported in presence of certain carboxylic and dicarboxylic acids which form stable complexes with iron, inhibiting H_2O_2 decomposition [34].

$$Fe + 2RCOOH \rightleftarrows Fe(RCOO)_2 + H_2 \quad \text{(Eq. 10)}$$

Given the potential of NAs to form iron complexes, CHA is likely to scavenge iron from the reaction media resulting in a lag phase which affects both H_2O_2 decomposition and CHA mineralization. To evaluate this, conditions related to the catalyst (pH, concentration, oxidation state) were varied in order to study the system's response.

Table 1
pH_0 influence on CHA mineralization. Experimental conditions: $[H_2O_2]_0 = 239$ mg/L; $[Fe^{2+}]$=20 mg/L; 280 W/m^2 irradiance; $T = 25$ °C; $r_{agit} = 250$ rpm, t: 240 min.

pH	X_{TOC} (%)	$-\overline{r_{TOC}} \times 10^2$(mg/L·min)
2.5	44.8	5.26
3	83.3	29
3.5	62.6	6.02

Table 2
Dissolved iron in solution. Experimental conditions: $[Fe^{2+}]_0 = 20$ mg/L; pH_0=3; $T = 25$ °C; 250 rpm, $[H_2O_2]_0 = 0$.

CHA (mg/L)	Total [Fe]	$[Fe^{2+}]$ (mg/L)
0	20.8	20.3
50	20.6	20.4

3.2. Influence of pH_0

When it comes to phenolic compounds degradation, it has been evidenced that pH around 3 is optimum for Fenton process regardless of target compound [35]. Nevertheless and given the lack of literature on Fenton degradation for NAs, influence of pH_0 was studied working at pH_0= 2.5, 3 and 3.5. Results are shown in Table 1.

As may be seen, optimum pH_0 is 3. In this conditions, hidroxi-Fe^{3+} complexes are more soluble and solution the predominant species is $Fe(OH)^{2+}$, which is the most photoactive. This interpretation is backed up by Malato et al., who proposed an optimum pH of 2.8 for the photo-Fenton process [36]. At pH higher than 3, mineralization reaction is retarded by Fe^{3+} precipitation as amorphous oxohydroxides (Fe_2O_3.nH_2O), while at inferior pH values, the delay of the reaction is related to an inhibition previous to Fe^{3+} complexation by H_2O_2 [37].

All runs presented in Table 1 suffered a slight acidification during the course of the reaction. For instance, in the $pH_0 = 3.5$ assay the final pH value was 3.22. This phenomenon is caused due to the generation of short-chain acids along the oxidation process [38].

3.3. Influence of catalyst concentration and oxidation state

Once the optimum pH_0 value was stablished, the catalyst concentration and the iron oxidation state were evaluated. Firstly, Fe^{2+} concentration was raised from 10 to 20 mg/L. This caused a great increase in the reaction rate (calculated from $t = 0$ to $t = 120$ min) from $-\overline{r_{TOC}}$= 0.11 mg/L·min to $-\overline{r_{TOC}}$= 0.29 mg/L·min. This result corroborates the hypothesis that CHA scavenges iron from reaction media. Nevertheless, Fe^{2+}dosage above 20 mg/L was not more effective, since precipitation in form of iron (III) hydroxide occurs [35]. Therefore optimum Fe^{2+} concentration was stablished at 20 mg/L.

To study the influence of oxidation state on the process, Fe^{2+} was substituted by Fe^{3+}, working in both cases at 20 mg/L. Using Fe^{3+}, a 77.9% TOC was reached in 120 min, which corresponds to a $-\overline{r_{TOC}}$= 0.21 mg/L·min, slightly slower than that observed for Fe^{2+}. Profile of TOC and H_2O_2 evolution depicted in Figure S2 of the SI shows a slightly higher lag phase in the case of Fe^{3+}, with similar final TOC and H_2O_2 conversion after 120 min reaction. Neyens and Baeyens reported this same effect, observing that the use of ferric salts instead of ferrous ones caused the Fenton reaction to occur more slowly [39]. Hence further experiments were performed at Fe^{2+}=20 mg/L.

In order to elucidate the interaction between CHA and iron, various experiments were carried out. CHA was mixed with an iron solution but without hydrogen peroxide, following the same conditions as those used during the reaction. The Dissolved iron was measured using to the o-phenanthroline method. Results are shown in Table 2. After 90 min exposure to LED light, these results remained invariable for both total Fe and Fe^{2+}. This suggests that the ligand between CHA and iron is a H_2O_2

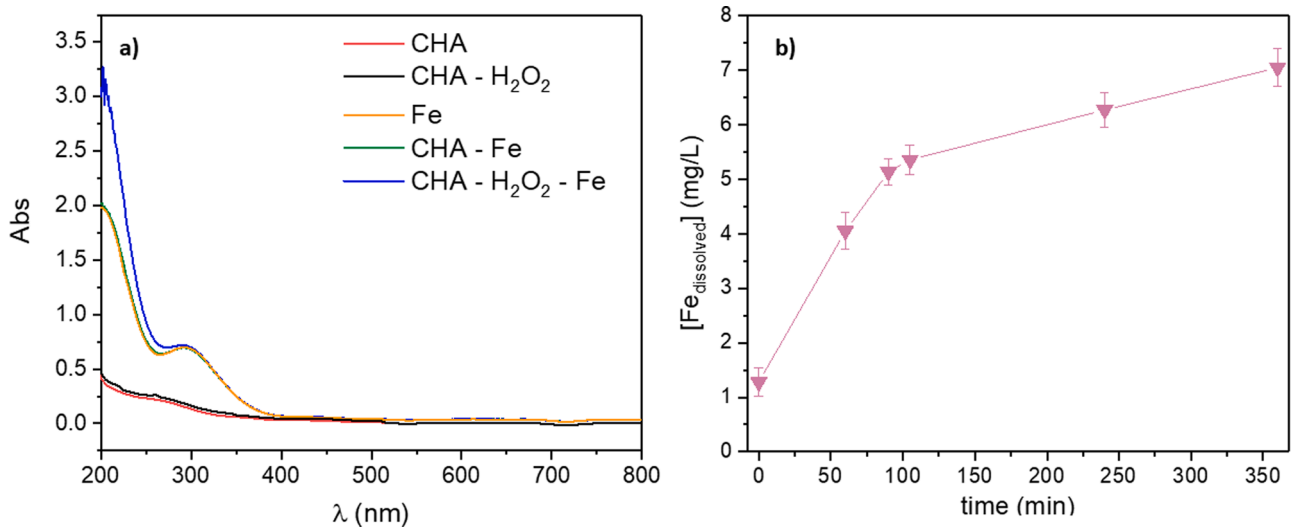

Fig. 2. a) changes in CHA spectra in presence of Fe and H_2O_2 and b) Dissolved Fe evolution in CHA photo-Fenton Experimental conditions: $[CHA]_0$ = 50 mg/L; $[H_2O_2]_0$ = 144 mg/L; $[Fe^{2+}]_0$ = 20 mg/L; 280 W/m^2 irradiance; pH_0=3; T = 25 °C; 250 rpm.

.

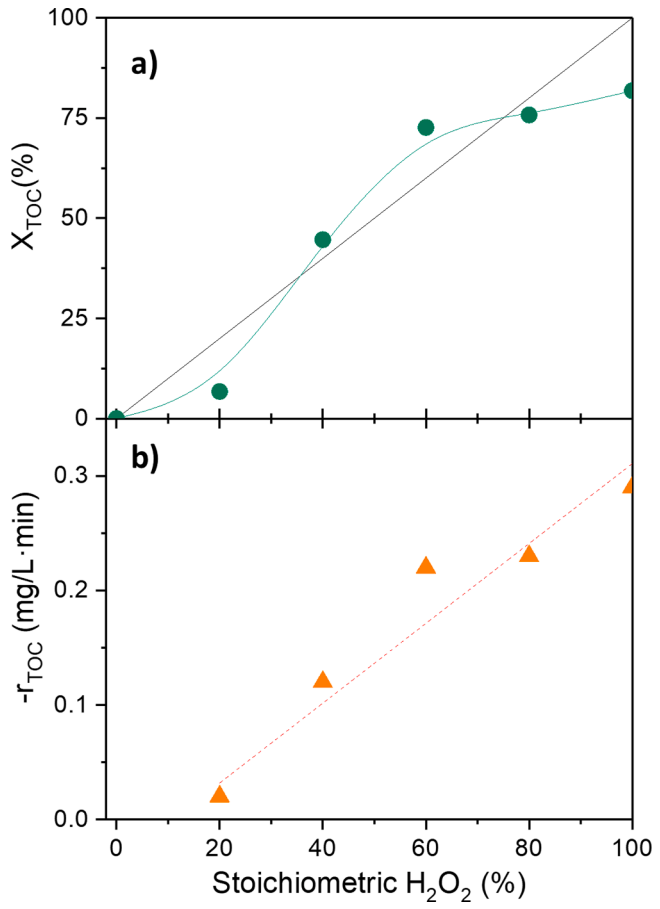

Fig. 3. a) TOC conversion and b) average mineralization rate and linearization (dotted line) of CHA at different H_2O_2 dosage. Experimental conditions: $[CHA]_0$ = 50 mg/L; $[Fe^{2+}]$=20 mg/L; 280 W/m^2 irradiance; pH_0=3; T = 25 °C; t :120 min, r_{agit}: 250 rpm.

molecule.

To gain further insight on the CHA-H_2O_2-Fe complex, spectrophotometric measurements of CHA by itself and in presence of iron and H_2O_2 were registered, as shown in Fig. 2a. As may be observed, the iron and CHA-Fe spectra are practically the same, suggesting a null interaction between these species. Nonetheless, when H_2O_2 is introduced in the system, the absorption in the UV region increases noticeably, confirming the formation of the CHA-H_2O_2-Fe complex.

Fig. 2b shows the Fe^{2+} evolution along the photo-Fenton degradation of CHA. Prior to H_2O_2 introduction in the system $[Fe^{2+}]_0$ was found to be 20.3 mg/L. After H_2O_2 addition, dissolved iron concentration decreased to 1.3 mg/L, due to the formation of the aforementioned complex. As the reaction proceeds, iron in solution rises, suggesting that vis-LED light incidence is able to break down the CHA-H_2O_2-Fe complex, making the Fe newly available in the reaction media for the Fenton process. This would explain the lag phase previously observed in Fig. 1b for CHA mineralization.

3.4. *Influence of H_2O_2 dose*

The main operational cost in the Fenton process is related to H_2O_2 [40]. Hence, the optimization of this reagent is crucial towards the development of cost-efficient technologies for water treatment. In this sense, CHA degradation was studied varying H_2O_2 concentration in a range of 20–100% in relation to stoichiometric amount for complete mineralization. Results on CHA mineralization and $-\overline{r_{TOC}}$ are depicted in Fig. 3. Focusing on Fig. 3a, the diagonal represents the ideal behavior for Fenton working at stoichiometric oxidant dose, where each fraction of converted H_2O_2 is employed in the elimination of the same amount of TOC [41]. As may be observed, at 60% the stoichiometric H_2O_2 dose, the mineralization degree is higher than that expected, with X_{TOC}: 74.9%. As can be observed in Fig. 3b., at this same H_2O_2 dose, the $-\overline{r_{TOC}}$ is higher than expected based on the linearization, represented by the dotted line. This is ascribed to the role of dissolved oxygen, which can react with organic radicals giving rise to the generation of HOO$^{\bullet}$, as shown in Eqs. (11)-(12) [42]. This effect has been also reported in the degradation of model naphthenic acids by persulfate oxidation [18]. In order to confirm the role of oxygen in the reaction, the 60% stoichiometric H_2O_2 run was repeated in an inert environment (N_2). Results shown in Figure S3 of the SI show a diminishment in the mineralization, with a final TOC removal of 57.6%. Hence, for subsequent runs the optimum H_2O_2 dosage was stablished at 60% the stoichiometric amount, which corresponds to 144 mg/L.

$$R^{\bullet} + O_2 \rightarrow RO_2^{\bullet} \quad \text{(Eq. 11)}$$

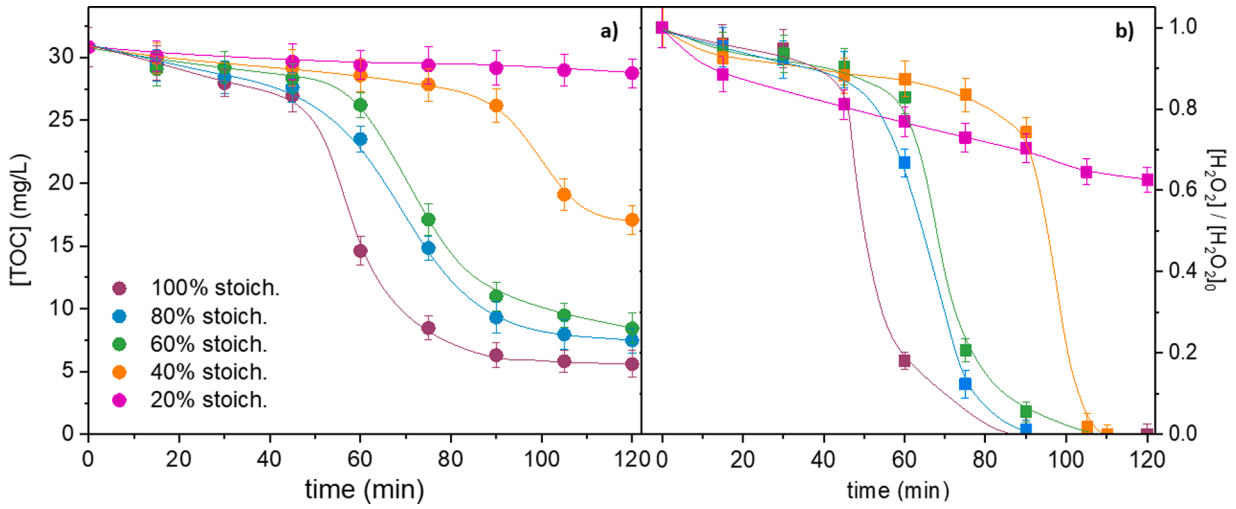

Fig. 4. a) TOC and b) H_2O_2 evolution in CHA photo-Fenton degradation. Experimental conditions : $[CHA]_0$ = 50 mg/L; $[Fe^{2+}]$=20 mg/L; 280 W/m^2 irradiance; pH_0=3; T = 25 °C; 250 rpm.

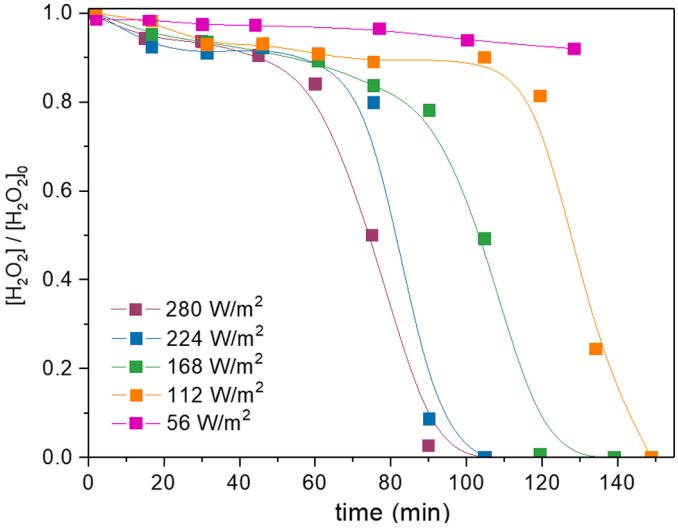

Fig. 5. H_2O_2 conversion dependence on irradiance. Experimental conditions: $[CHA]_0$ = 50 mg/L; $[Fe^{2+}]$=20 mg/L; $[H_2O_2]_0$ = 144 mg/L; pH_0=3; T = 25 °C; 250 rpm.

$$RO_2^{\bullet} + H_2O_2 \rightarrow CO_2 + R'H + HOO^{\bullet} \quad \text{(Eq. 12)}$$

Also TOC and H_2O_2 evolution along the reaction were evaluated, as seen in Fig. 4. As H_2O_2 dose is increased, its decomposition lag phase is shortened, and the overall oxidant consumption rate is faster, which also affects the mineralization of CHA. Furthermore, at 20% H_2O_2 stoichiometric dose, oxidant consumption is incomplete. This trend reconfirms the proposed mechanism for the reaction based on the formation of CHA-H_2O_2-Fe complex. In dark conditions, further H_2O_2 decomposition is very slow, since all Fe is complexed, hindering the H_2O_2 decomposition into oxidant radicals, and therefore CHA mineralization. In presence of UV–vis radiation, CHA-H_2O_2-Fe breaks down, iron is newly available for H_2O_2 decomposition and pollutant mineralization occurs. The rate increases according to the amount of oxidant in the medium. Considering this mechanism, working at H_2O_2 dosages lower than 33% of the stoichiometric amount (47.5 mg/L), only the CHA-H_2O_2-Fe formation takes place, leading to a practically null mineralization, as previously seen in Fig. 3a. On the other hand, if there is a high concentration of hydrogen peroxide, the radicals produced in its decomposition can compete with each other, causing the mineralization

Table 3
Rate constants for H_2O_2 decomposition in photoassisted Fenton process.

Irradiance (W/m^2)	$k_{app} \times 10^1$ (min^{-1})	r^2
56	0.05 ± 0.002	0.984
112	1.51 ± 0.02	0.992
168	1.46 ± 0.07	0.914
224	1.48 ± 0.03	0.989
280	1.46 ± 0.05	0.943

Table 4
Influence of irradiance on TOC mineralization Experimental conditions: $[CHA]_0$ = 50 mg/L; $[H_2O_2]_0$ = 144 mg/L; $[Fe^{2+}]$=20 mg/L; pH=3; T = 25 °C; 250 rpm.

Irradiance (W/m^2)	Lag time (min)	Mineralized TOC (%)
56	135 ± 1.7	15.7
112	120 ± 1.2	71.2
168	90 ± 0.8	74.3
224	75 ± 1.3	74.8
280	65 ± 1.8	74.9

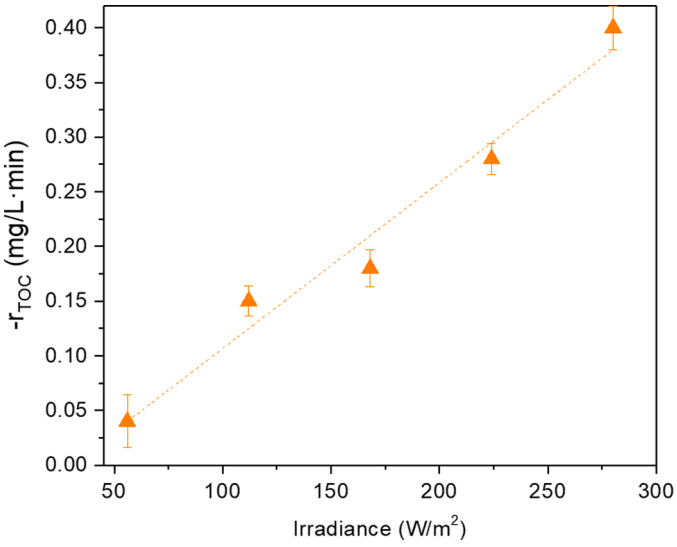

Fig. 6. Average TOC degradation rate dependence on radiant flux. Experimental conditions: $[CHA]_0$ = 50 mg/L; $[Fe^{2+}]$=20 mg/L; $[H_2O_2]_0$ = 144 mg/L; pH_0=3; T = 25 °C; 250 rpm.

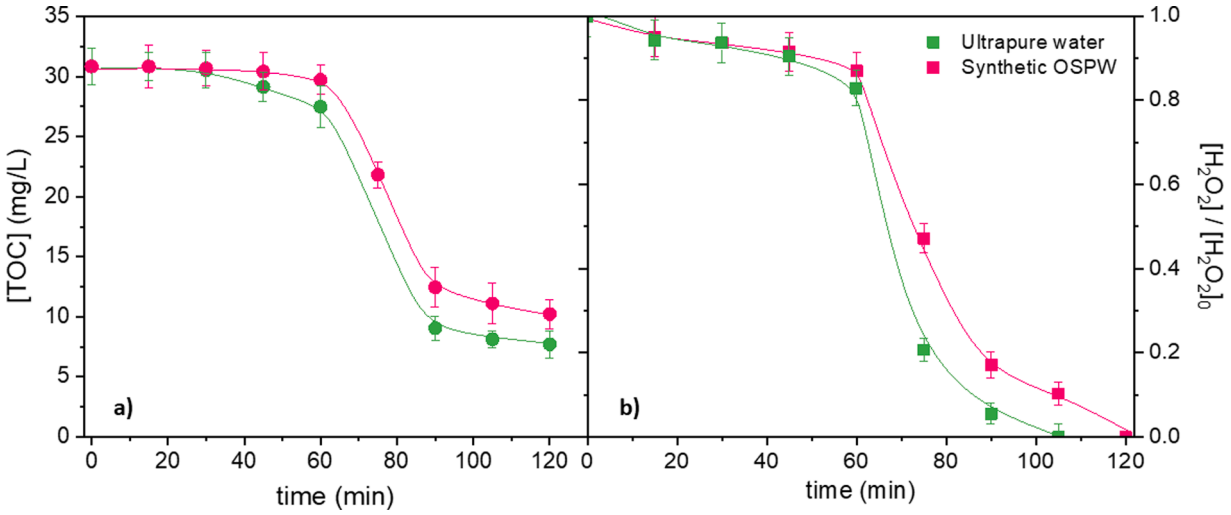

Fig. 7. Influence of the water matrix in a) CHA mineralization and b) H_2O_2 consumption by photo-Fenton. Experimental conditions: $[CHA]_0$ = 50 mg/L; $[H_2O_2]_0$ = 144 mg/L; $[Fe^{2+}]$=20 mg/L; 280 W/m^2 irradiance; pH_0=3; T = 25 °C; 250 rpm.

process to slow down, as can also be seen in Fig. 3.

3.5. Influence of radiant flux

Once obtained the optimum H_2O_2 dosage, influence of the radiant flux on the Fenton process was evaluated. Fig. 5 shows the H_2O_2 along the reaction. After the initial lag phase, H_2O_2 decomposition kinetics follows a pseudo-first order with an apparent rate constant k_{app}: 0.15 min^{-1} for practically all the radiant fluxes applied, as collected in Table 3. When radiant flux is lower than 56 W/m^2, the CHA-H_2O_2-Fe breakdown is very slow. This is also translated in a diminished mineralization degree, as shown in Table 4.

Regarding pollutant depletion, the higher the radiant flux, the higher the $-\overline{r_{TOC}}$ is, as seen in Fig. 6. At radiant flux above 56 W/m^2, a mineralization degree higher than 70% is reached in all cases. Still, the incident flux has a great effect on the lag phase and thus, on the kinetics. In this sense, augmenting the flux from 112 to 280 W/m^2, the lag phase is diminished by two-fold, allowing complete H_2O_2 consumption at t: 110 min with 74.9% TOC removal.

3.6. Effect of the water matrix

The effect of the water matrix can greatly influence the oxidation processes [26]. Hence, it is necessary to assess the feasibility of the photo-Fenton process in CHA mineralization in a water matrix with a higher complexity than that of ultrapure water. OSPW presents a complex composition, which is characterized by its moderate salinity, as reported elsewhere [43–45]. Attending to the usual composition of OSPW, a synthetic matrix was produced by addition of [NaCl] = 360 mg/L, [Na_2SO_4] = 120 mg/L and [Na_2CO_3] = 440 mg/L to the usual CHA solution. Results for CHA mineralization and H_2O_2 evolution in ultrapure water and synthetic OSPW working at 60% the stoichiometric H_2O_2 dose can be found in Fig. 7. As can observed, the presence of inorganic salts diminishes slightly the process efficiency, probably due to HO$^\bullet$ scavenging [26]. Still, CHA is efficiently mineralized with a 66% TOC removal in the synthetic OSPW matrix, against 75% in ultrapure water. Hence, despite the scavenging effect, the photo-Fenton process using vis-LED radiation is a feasible technology for the degradation of naphthenic acids.

Conclusions

Vis-LED assisted Fenton is feasible for the degradation of CHA. The process undergoes a complex mechanism where H_2O_2 acts as both oxidant and link for the generation of a CHA-H_2O_2-Fe complex, which produces a lag phase in CHA photo-Fenton degradation. In absence of light, the generation of this specie implies the end of the reaction, as no further H_2O_2 decomposition can take place. On the other hand, when applying a radiant flux above 56 W/m^2, the CHA-H_2O_2-Fe complex is photoactivated, allowing further H_2O_2 decomposition and the effective mineralization of CHA. H_2O_2 dose and radiation flux were found to be the most determining parameters affecting CHA mineralization. The system requires a minimum H_2O_2 dose of 33% the stoichiometric dose to enable the complex breakdown. Working at 60% the stoichiometric dose (H_2O_2 = 144 mg/L) TOC conversion is higher than that predicted by the stoichiometry of the reaction, due to the role of dissolved oxygen in the pollutant degradation. Additionally, the radiation flux was found to be determining in the process kinetics, playing a key role in the photoactivation of the CHA-OH-Fe complex and the duration of the initial lag phase. Finally, the effect of the water matrix was addressed, finding a slight diminishment in the process efficiency in simulated OSPW, with a 66% mineralization against 75% when working in ultrapure water.

Authors' contribution

Alicia L. Garcia-Costa: investigation, data curation, writing: original draft, Lucia Lopez-Perela: conceptualization, investigation, data curation, methodology, writing: original draft, Gema Pliego: writing: review, Juan A. Zazo: funding acquisition, writing: review, Jose A. Casas: formal analysis, funding acquisition, supervision, writing: review and editing.

Declaration of Competing interests

The authors declare that they have no known competing financial interests or personal relationships that could have appeared to influence the work reported in this paper.

Acknowledgments

Authors would like to thank the Comunidad de Madrid for the financial support received through project P2018/EMT-4341 REMTAVARES-CM.

Supplementary materials

Supplementary material associated with this article can be found, in the online version, at doi:10.1016/j.ceja.2021.100198.

References

[1] C.C. Wu, A. De Visscher, I.D. Gates, On naphthenic acids removal from crude oil and oil sands process-affected water, Fuel 253 (2019) 1229–1246.
[2] R. Qin, Z.T. How, M.C. El-Din, Photodegradation of naphthenic acids induced by natural photosensitizer in oil sands process water, Water Res 164 (2019) 8.
[3] NRDC, https://environmentaldefence.ca/report/albertas-tailings-ponds/, 2017.
[4] A. Pinzon-Espinosa, R. Kanda, Naphthenic acids are key contributors to toxicity of heavy oil refining effluents, Sci. Total Environ. 729 (2020) 10.
[5] F.M. Holowenko, M.D. MacKinnon, P.M. Fedorak, Characterization of naphthenic acids in oil sands wastewaters by gas chromatography-mass spectrometry, Water Res 36 (2002) 2843–2855.
[6] L.T. Hendges, T.C. Costa, B. Temochko, S.Y.G. Gonzalez, L.P. Mazur, B.A. Marinho, A. da Silva, S.E. Weschenfelder, A.A.U. de Souza, S. de Souza, Adsorption and desorption of water-soluble naphthenic acid in simulated offshore oilfield produced water, Process Saf. Environ. Protect. 145 (2021) 262–272.
[7] Y. Rashed, S.A. Messele, H.B. Zeng, M.G. El-Din, Mesoporous carbon xerogel material for the adsorption of model naphthenic acids: structure effect and kinetics modelling, Environ. Technol. 41 (2020) 3534–3543.
[8] H. Liang, C.J. Zou, Adsorption of naphthenic acids from oil sand process-affected water with water-insoluble poly(beta-cyclodextrin-citric acid), Can. J. Chem. Eng. 97 (2019) 1894–1902.
[9] O.T. Ore, A.O. Adeola, Toxic metals in oil sands: review of human health implications, environmental impact, and potential remediation using membrane-based approach, Energy Ecol. Environ. 6 (2021) 81–91.
[10] H. Liang, C.J. Zou, W.Y. Tang, Development of novel polyether sulfone mixed matrix membranes to enhance antifouling and sustainability: treatment of oil sands produced water (OSPW), J. Taiwan Inst. Chem. Eng. 118 (2021) 215–222.
[11] A. Alpatova, E.S. Kim, S.M. Dong, N. Sun, P. Chelme-Ayala, M.G. El-Din, Treatment of oil sands process-affected water with ceramic ultrafiltration membrane: effects of operating conditions on membrane performance, Sep. Purif. Technol. 122 (2014) 170–182.
[12] A.L. Garcia-Costa, L. Lopez-Perela, X.Y. Xu, J.A. Zazo, J.J. Rodriguez, J.A. Casas, Activated carbon as catalyst for microwave-assisted wet peroxide oxidation of aromatic hydrocarbons, Environ. Sci. Pollut. Res. 25 (2018) 27748–27755.
[13] X.Y. Xu, G. Pliego, J.A. Zazo, S.B. Sun, P. Garcia-Munoz, L. He, J.A. Casas, J. J. Rodriguez, An overview on the application of advanced oxidation processes for the removal of naphthenic acids from water, Crit. Rev. Environ. Sci. Technol. 47 (2017) 1337–1370.
[14] A.K.H. Al jibouri, J.N. Wu, S.R. Upreti, Heterogeneous catalytic ozonation of naphthenic acids in water, Can. J. Chem. Eng. 97 (2019) 67–73.
[15] A.S. Abdalrhman, C.J. Wang, Z.T. How, M.G. El-Din, Degradation of cyclohexanecarboxylic acid as a model naphthenic acid by the UV/chlorine process: kinetics and by-products identification, J. Hazard. Mater. 402 (2021) 9.
[16] Z. Fang, R.F. Huang, Z.T. How, B. Jiang, P. Chelme-Ayala, Q. Shi, C.M. Xu, M.G. El-Din, Molecular transformation of dissolved organic matter in process water from oil and gas operation during UV/H2O2, UV/chlorine, and UV/persulfate processes, Sci. Total Environ. 730 (2020) 8.
[17] X.Y. Xu, G. Pliego, A.L. Garcia-Costa, J.A. Zazo, S.M. Liu, J.A. Casas, J.J. Rodriguez, Cyclohexanoic acid breakdown by two-step persulfate and heterogeneous Fenton-like oxidation, Appl. Catal. B-Environ. 232 (2018) 429–435.
[18] X.Y. Xu, G. Pliego, J.A. Zazo, J.A. Casas, J.J. Rodriguez, Mineralization of naphtenic acids with thermally-activated persulfate: the important role of oxygen, J. Hazard. Mater. 318 (2016) 355–362.
[19] A. Pinzon-Espinosa, T.J. Collins, R. Kanda, Detoxification of oil refining effluents by oxidation of naphthenic acids using TAML catalysts, Sci. Total Environ. 784 (2021) 10.
[20] N. Negreira, J. Regueiro, M.L. de Alda, D. Barcelo, Transformation of tamoxifen and its major metabolites during water chlorination: identification and in silico toxicity assessment of their disinfection byproducts, Water Res 85 (2015) 199–207.
[21] J.A. Zazo, J.A. Casas, A.F. Mohedano, M.A. Gilarranz, J.J. Rodriguez, Chemical pathway and kinetics of phenol oxidation by Fenton's reagent, Environ. Sci. Technol. 39 (2005) 9295–9302.
[22] R. Munter, Advanced oxidation processes – current status and prospects, Proc. Estonian Acad. Sci. Chem. 50 (2001) 59–80.
[23] M.D. Marchetti, E.B. Azevedo, Degradation of NSAIDs by optimized photo-Fenton process using UV-LEDs at near-neutral pH, J. Water Process. Eng. 35 (2020) 8.
[24] G. Pliego, P. Garcia-Munoz, J.A. Zazo, J.A. Casas, J.J. Rodriguez, Improving the Fenton process by visible LED irradiation, Environ. Sci. Pollut. Res. 23 (2016) 23449–23455.
[25] A.L. Garcia-Costa, A. Sarabia, J.A. Zazo, J.A. Casas, UV-assisted Catalytic Wet Peroxide Oxidation and adsorption as efficient process for arsenic removal in groundwater, Catal. Today 361 (2021) 176–182.
[26] A.L. Garcia-Costa, J.E. Silveira, J.A. Zazo, D.D. Dionysiou, J.A. Casas, Graphite as catalyst for UV-A LED assisted catalytic wet peroxide oxidation of ibuprofen and diclofenac, Chem. Eng. J. Adv. 6 (2021), 100090.
[27] Y. Zhang, N. Klamerth, P. Chelme-Ayala, M. Gamal El-Din, Comparison of classical fenton, nitrilotriacetic acid (NTA)-Fenton, UV-Fenton, UV photolysis of Fe-NTA, UV-NTA-Fenton, and UV-H2O2 for the degradation of cyclohexanoic acid, Chemosphere 175 (2017) 178–185.
[28] G.M. Eisenberg, Colorimetric determination of hydrogen peroxide, Ind. Eng. Chem.-Anal. Ed. 15 (1943) 327–328.
[29] S.E.Q. Ashley, Colorimetric determination of traces of metals. By E. B. Sandell, J. Phys. Chem. 49 (1945) 263–264.
[30] J.B. De Heredia, J. Torregrosa, J.R. Dominguez, J.A. Peres, Kinetic model for phenolic compound oxidation by Fenton's reagent, Chemosphere 45 (2001) 85–90.
[31] G. Czapski, A. Samuni, D. Meisel, Reactions of organic radicals formed by some "Fenton-like" reagents, J. Phys. Chem. 75 (1971) 3271–3280.
[32] F. Gozzo, Radical and non-radical chemistry of the Fenton-like systems in the presence of organic substrates, J. Mol. Catal. A: Chem. 171 (2001) 1–22.
[33] P. Jin, W. Robbins, G. Bota, Kinetic reaction modeling of naphthenic acid corrosion and Sulfidation in refineries-a mechanistic model, Corrosion 74 (2018) 1351–1362.
[34] D. Hermosilla, M. Cortijo, C.P. Huang, The role of iron on the degradation and mineralization of organic compounds using conventional Fenton and photo-Fenton processes, Chem. Eng. J. 155 (2009) 637–646.
[35] G. Pliego, J.A. Zazo, P. Garcia-Munoz, M. Munoz, J.A. Casas, J.J. Rodriguez, Trends in the intensification of the fenton process for wastewater treatment: an overview, Crit. Rev. Environ. Sci. Technol. 45 (2015) 2611–2692.
[36] S. Malato, P. Fernandez-Ibanez, M.I. Maldonado, J. Blanco, W. Gernjak, Decontamination and disinfection of water by solar photocatalysis: recent overview and trends, Catal. Today 147 (2009) 1–59.
[37] J.J. Pignatello, Dark and photoassisted Fe3+-catalyzed degradation of chlorophenoxy herbicides by hydrogen peroxide, Environ. Sci. Technol. 26 (1992) 944–951.
[38] A.L. Garcia-Costa, A. Luengo, J.A. Zazo, J.A. Casas, Cutting oil-water emulsion wastewater treatment by microwave assisted catalytic wet peroxide oxidation, Sep. Purif. Technol. 257 (2021).
[39] E. Neyens, J. Baeyens, A review of classic Fenton's peroxidation as an advanced oxidation technique, J. Hazard. Mater. 98 (2003) 33–50.
[40] A.L. Garcia-Costa, J. Carbajo, R. Masip, A. Quintanilla, F.J. Yuste-Cordoba, J. A. Casas, Enhanced cork-boiling wastewater treatment by electro-assisted processes, Sep. Purif. Technol. 241 (2020) 6.
[41] A.L. Garcia-Costa, J.A. Zazo, J.J. Rodriguez, J.A. Casas, Intensification of catalytic wet peroxide oxidation with microwave radiation: activity and stability of carbon materials, Sep. Purif. Technol. 209 (2019) 301–306.
[42] C. vonSonntag, P. Dowideit, X.W. Fang, R. Mertens, X.M. Pan, M.N. Schuchmann, H.P. Schuchmann, The fate of peroxyl radicals in aqueous solution, Water Sci. Technol. 35 (1997) 9–15.
[43] S.M. Dong, E.S. Kim, A. Alpatova, H. Noguchi, Y. Liu, M.G. El-Din, Treatment of oil sands process-affected water by submerged ceramic membrane microfiltration system, Sep. Purif. Technol. 138 (2014) 198–209.
[44] P. Pourrezaei, P. Drzewicz, Y. Wang, M. Gamal El-Din, L.A. Perez-Estrada, J. W. Martin, J. Anderson, S. Wiseman, K. Liber, J.P. Giesy, The impact of metallic coagulants on the removal of organic compounds from oil sands process-affected water, Environ. Sci. Technol. 45 (2011) 8452–8459.
[45] E.-S. Kim, Y. Liu, M. Gamal El-Din, The effects of pretreatment on nanofiltration and reverse osmosis membrane filtration for desalination of oil sands process-affected water, Sep. Purif. Technol. 81 (2011) 418–428.